J. Fluid Mech. (1975), *vol.* 72, *part* 3, *pp.* 455–480
Printed in Great Britain

Conditionally sampled measurements in a heated turbulent jet

By R. A. ANTONIA, A. PRABHU AND S. E. STEPHENSON

Department of Mechanical Engineering, University of Sydney, New South Wales 2006, Australia

(Received 13 December 1974)

Measurements of velocity fluctuations u (axial) and v (radial) and temperature fluctuations θ averaged over the turbulent zone have been made in a turbulent heated jet with a co-flowing stream and compared with the conventionally averaged results. The zone-averaged mean temperature and temperature fluctuation intensity appear to be nearly homogeneously distributed in the outer, intermittent region of the jet. This homogeneity does not apply to the u and v fluctuations. The flatness factor of the temperature within the turbulent part of the flow is remarkably constant throughout the intermittent region. Although the skewness of the turbulent θ fluctuations is non-zero, it is smaller than the skewness of the turbulent u and v fluctuations. The average $\overline{\theta v}$ of the heat flux over the turbulent zone increases in the intermittent region whereas the zone-averaged momentum flux $\overline{uv}$ and zone-averaged heat flux $\overline{\theta u}$ continuously decrease. This leads to the Prandtl number of the turbulent fluid being smaller than the conventional Prandtl number in the outer part of the flow. A budget for the square of the temperature fluctuations within the turbulent part of the flow indicates a constant distribution of temperature dissipation. The transport of heat by the large-scale structure of the flow is briefly discussed in the light of available experimental information on other turbulent shear flows.

1. Introduction

One of the most important features of any turbulent flow is the complex interaction that occurs between its large- and small-scale structure. A study of the small-scale velocity and temperature fluctuations for a heated round turbulent jet with a co-flowing stream was initiated by Antonia & Van Atta (1975). A strong correlation was observed between the dissipation fields of velocity and temperature fluctuations and the influence of this correlation on the small-scale properties of the flow was investigated. The anisotropy of the small-scale temperature field was highlighted by the non-zero skewness of the temperature derivative. This result has also been noted by Freymuth & Uberoi (1971, 1973) for two-dimensional and axisymmetric wakes and by Gibson, Friehe & McConnell (1974, private communication) for heated axisymmetric jets and wakes. Gibson *et al.* suggested that this anisotropy might be the residual effect

of a large-scale temperature field one of whose characteristic features is a ramp-like temperature distribution, especially in the intermittent part of the flow. The point of highest temperature of the ramp, usually associated with a sharp thermal gradient, may occur at either the downstream or upstream end of the turbulent/irrotational interface depending on the sign of the vorticity of the main flow.

The purpose of this paper is to present some experimental information relating to the large-scale structure of a heated round jet with a co-flowing stream. The large-scale features of the flow are determined with respect to the passage of the interface, conveniently defined in this case by observation of the passive temperature contaminant in the flow. LaRue & Libby's (1974*a*) experiment in the turbulent wake of a heated cylinder has shown that the interface is related primarily to the large-scale structure of the flow field. In this paper, properties of the velocity and temperature fluctuations within the turbulent part only of the flow obtained across the jet using experimental techniques similar to those of Kovasznay, Kibens & Blackwelder (1970) and Wygnanski & Fiedler (1970) are reported and compared with the conventionally averaged properties. The selection of these properties presented in §§ 3–6 includes the moments up to the fourth order of the velocity fluctuations u (in the axial direction x) and v (in the radial direction r) and temperature fluctuations θ and also the cross-correlations $\overline{u\theta}$, $\overline{uv}$ and $\overline{v\theta}$. Also, a budget of the square of the temperature fluctuations within the turbulent regions is compared with the more conventional budget. The results pertaining to the large-scale transport of heat and momentum in this flow are compared with results obtained in other shear flows.

2. Experimental conditions and techniques

The jet rig used has been described in Antonia & Bilger (1973). The jet is supplied from the laboratory air supply and heated electrically before entering a 50 mm diameter supply pipe which contracts to the diameter $d = 20{\cdot}3$ mm of the stainless-steel nozzle used in this investigation. At the nozzle exit the jet temperature was maintained at approximately 34 °C above the ambient temperature. The jet velocity U_j was kept constant at about 32 m s^{-1} for all the experiments, this velocity being continuously checked by monitoring the pressure drop across an orifice plate inserted in the laboratory air supply pipe upstream of the heater section. The external air was supplied by a centrifugal blower and was effectively at the ambient temperature (approximately 15 °C). Three values of the external velocity U_1 were used in this investigation, corresponding to nominal values of the ratio U_j/U_1 of 6·6, 2·9 and 1·9 respectively.†

The mean and fluctuating temperatures were obtained with a platinum/10 % rhodium wire of length 1 mm and diameter 1 μm. The velocity fluctuations u and v were measured with a miniature DISA 55 X-probe which had two platinum-coated tungsten wires of length 1 mm and diameter 5 μm. The wires were welded on to prongs attached to the quartz body of the probe and were mounted with

† The majority of the results presented in the following sections correspond to $U_j/U_1 = 6{\cdot}6$.

a separation of less than 1 mm at approximately 90° to each other. The 1 μm diameter temperature sensor or 'cold' wire was kept horizontal and normal to the axial flow direction and was situated approximately 1 mm below the geometrical centre of the vertical X-wire array. A total-head tube of diameter 1 mm was mounted with its axis parallel to the jet axis and its mouth located a distance of about 1 mm from the centre of the X-array in the lateral direction. The static pressure was constant across the jet cross-section for any given x and was measured at a tapping on the sliding roof of the working section. The dynamic pressure was recorded on a MENSOR pressure gauge.

The temperature wire, of resistance approximately 125 Ω, was operated with a constant-current anemometer described in Stellema, Antonia & Prabhu (1975) at a current of 0·2 mA. The thermal coefficient of resistivity α of the 'cold' wire was obtained by mounting the cold wire next to a copper–constantan thermocouple in the potential core of a jet (7·2 cm diameter nozzle) which is part of another calibration rig. The e.m.f. of the thermocouple was measured on a Cambridge potentiometer. The value of α for the wire used was estimated to be 0·0034 °C^{-1}.

The X-probe wires were operated with two sets of DISA 55 MO1/55M10 constant-temperature anemometers at an overheat ratio of 0·8. The anemometer outputs were fed into two DISA 55 D26 signal conditioners with the frequency response set at d.c.–8 kHz. The conditioners were used to suppress the d.c. component of the anemometer outputs and to amplify these signals for their efficient recording on a Hewlett-Packard 3525 A FM tape transport. Also recorded with the X-wire signals were the d.c. and a.c. temperature signals. The a.c. signal was recorded directly while the d.c. signal was recorded via a DISA 55 D 26 signal conditioner, once again to achieve a good signal-to-noise ratio on the recorder. The recorded temperature signals were compensated for the thermal inertia of the wire with a compensator designed to give a frequency response flat up to 20 kHz. The time constant of the wire was estimated by observing on a storage oscilloscope the response of the cold wire to the crossing of the interface in the outer, intermittent region of the heated jet. The temperature jump at the leading (or downstream) end of the interface was assumed to be sharp. The -3 dB point of the wire determined in this way was typically 0·13 ms at a speed $U = 8\,\mathrm{m\,s^{-1}}$. The time constant was checked before and after each experimental run as the relationship between the time constant and the speed was found to be significantly affected by ageing of the wire. Records of typically 80 s duration were established on the analog tape recorder at a speed of 38·1 cm s^{-1}, at which the recorder frequency response was flat up to 5 kHz (-3 dB point).

For small u and θ fluctuations the voltages for the hot and cold wires are given approximately by

$$e_{1h} = a_1 u + b_1 v + c_1 \theta, \quad e_{2h} = a_2 u + b_2 v + c_2 \theta, \tag{1), (2}$$

$$e_c = a_3 u + c_3 \theta. \tag{3}$$

The sensitivity coefficients a_1, b_1, a_2, b_2, c_1 and c_2 for the X-wire were determined

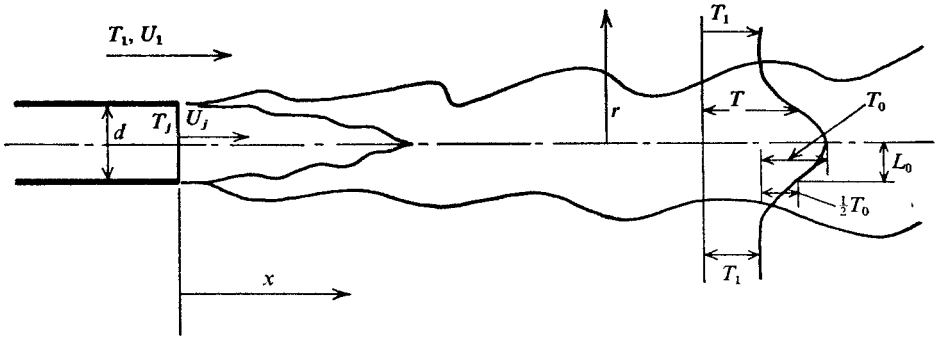

FIGURE 1. Schematic diagram of jet and co-ordinate axes.

by a speed-and-yaw calibration of the wire in the isothermal co-flowing stream and an assumed heat balance equation of the form

$$I^2R_w = (A + BU^m)(T_w - T_a),$$

where I is the probe current, R_w the wire resistance, U the velocity normal to the wire and T_w and T_a are the wire and local ambient temperatures respectively. From the above heat-transfer relation the coefficients a_1, b_1, c_1, etc., were calculated using (for small values of temperature variations across the jet)

$$a = \partial E/\partial U \simeq \partial E_1/\partial U, \quad c = \partial E/\partial T \simeq \tfrac{1}{2}\beta E,$$

where $\beta = -\alpha R_1/(R_w - R_1)$ and E_1 is the wire voltage at the ambient external-stream temperature T_1. The defect temperature T_0 was 2·43 °C for $U_j/U_1 = 6{\cdot}6$ at $x/d = 59$. For this value of T_0, the estimated error in a, b and c is approximately 0·8 % if we use the isothermal calibration.

The velocity sensitivity a_3 of the cold wire was (for the present experimental conditions) estimated to be about 0·0018 °C/m s^{-1}, using Wyngaard's (1971) expression. This sensitivity was neglected as it leads to errors in $\overline{u\theta}$ and $\overline{v\theta}$ of about 1 % for turbulence levels $\overline{(u^2)}^{\frac{1}{2}}/U_0$ or $\overline{(v^2)}^{\frac{1}{2}}/U_0 \simeq 0{\cdot}25$. Wyngaard estimated that, for isotropic turbulence, the velocity sensitivity leads to an overestimation of $\overline{(\partial\theta/\partial x)^2}$ by 1 %.

To determine u and v, the tape-recorder signals e_{1h} and e_{2h} were played back through operational-amplifier dual summers on an EAI 180 analog computer. Velocity contamination of these signals was removed by subtracting $c_1\theta$ and $c_2\theta$ from e_{1h} and e_{2h}. Equations (1) and (2) were then solved with the aid of an analog circuit which consisted of six operational amplifiers and four calibrated potentiometers set to the values of a_1, a_2, b_1 and b_2. The outputs u and v of this circuit were then used, together with the θ signal, as inputs to a multiplier to obtain the products $u\theta$, uv and $v\theta$. The mean values of these signals were obtained with a P.A.R. box car integrator Model CW-1 with an effective integration time of 10–100 s. When forming u^2, θ^2 and v^2 the instantaneous squared output of the DISA 55 D35 r.m.s. meter was fed into the box car integrator operated in the continuous mode. A multiplier was also used instead of the r.m.s. meter. Multipliers on the EAI 180 were used only when the third- and fourth-order

moments of u, v and θ were required, for the formation of the skewness and flatness factors presented in § 6. The co-ordinate axes used in this paper are shown in figure 1.

3. Conditional measurements

The only conditional type of measurement attempted here is the turbulent zone average, namely the average of a quantity over the turbulent region of the flow only. Adopting the same convention as in Antonia (1972), the zone average of a quantity Q is defined by $\bar{Q}_t = \overline{IQ}/\bar{I}$, where the subscript t indicates that the averaging is carried out over the turbulent zone only and $I(t)$ is the intermittency function, set to one when the flow is turbulent and to zero when it is irrotational. The value of $\bar{I}$ is clearly the intermittency factor γ, whilst the average frequency of $I(t)$ is referred to as f_γ, the mean crossing frequency of the interface. The difficulties in making accurate determinations of $\bar{Q}_t$ result from the difficulties in forming $I(t)$ objectively. Some of these difficulties have been described in Antonia & Atkinson (1974) and in Bradshaw & Murlis (1973). In the present study $I(t)$ was obtained by considering only the temperature signal, as in the case of Kovasznay & Ali (1974) and LaRue & Libby (1974*b*). Whenever the instantaneous temperature in the jet was higher than the ambient air temperature the flow was considered turbulent. More accurately, $I(t)$ was set to 1 whenever the local temperature $T(t)$ exceeded $T_1 + T_H$, where the introduction of the threshold T_H was necessary to allow for the noise level of the anemometer signal. In the generation of $I(t)$ from a detector function based on $u(t)$ or the derivative $\partial u/\partial t$ (e.g. by Kovasznay *et al.* 1970) a hold time was required in addition to the threshold in order to avoid spurious indications of irrotational regions in a turbulent flow patch and vice versa. In the present case, no hold time was required,† and it is felt that the removal of this parameter from the generation of $I(t)$ leads to a more satisfactory determination of f_γ, which is particularly sensitive to the setting of this hold time (Antonia & Atkinson 1974). As the d.c. temperature signal was used, the threshold was kept constant for most of the traverse across the jet but was varied slightly as the centre of the jet was neared. The value of T_H was set by visual inspection of $\theta(t)$ and $I(t)$ on a storage oscilloscope.

The effect of varying the threshold on the values of γ and f_γ is shown in figure 2 for $x/d = 59$, $U_j/U_1 = 6{\cdot}6$ and three values of $\eta = r/L_0$ (0·89, 1·33 and 1·63) for which the visual inspection setting gave γ as 0·89, 0·45 and 0·11 respectively. These three values were selected as representative values for high, medium and low γ. At low and medium γ the γ distributions show, as can be expected, a sharp change with threshold setting, increasing sharply as the threshold setting becomes less than the noise level of the amplifier, whereas the variation is gradual at high γ. It should be noted that there exists no plateau where γ is reasonably constant.

† Although Kovasznay & Ali (1974) used the temperature signal as their indicator function, they also used a non-zero hold time. Sunyach & Mathieu (1969) used $(\partial\theta/\partial t)^2$ for the determination of γ in a heated two-dimensional mixing layer. They claimed that the differentiation of θ removes the difficulty of spurious ambient-temperature fluctuations. The use of $\partial\theta/\partial t$ does however reintroduce the more difficult problem of setting a hold time.

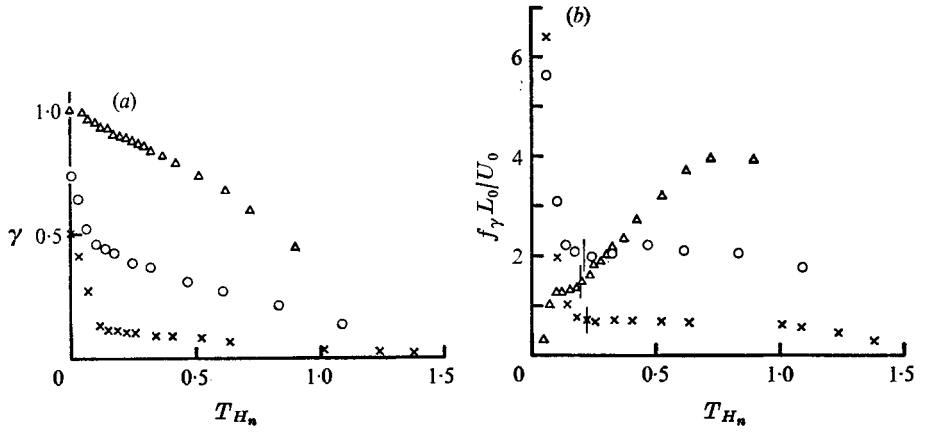

FIGURE 2. Effect of threshold T_{H_n} on γ and f_γ ($U_j/U_1 = 6{\cdot}6$). T_{H_n} is defined as $T_H/[\overline{(\theta-\overline{\theta}_n)_t^2}]^{\frac{1}{2}}$.

Vertical lines indicate visual settings of T_H. (a) γ; (b) f_γ. ×, $\gamma = 0{\cdot}11, \eta = 1{\cdot}63$; ○, $\gamma = 0{\cdot}40$, $\eta = 1{\cdot}33$; △, $\gamma = 0{\cdot}88$, $\eta = 0{\cdot}89$.

The variation of $f(\gamma)$ shows remarkably different trends at different γ, also increasing very rapidly as the threshold falls below the noise level for low and medium γ and decreasing rapidly to zero for high γ. In all three cases it is possible to identify a plateau region just after the sharp increase or decrease in $f(\gamma)$. The visual setting of the threshold falls at the beginning of this plateau for low and medium γ and at end of this plateau for high γ. After this plateau, f_γ increases and then finally decreases with the threshold setting for high and medium γ. These curves thus suggest that an intermittency based on $\theta(t)$ has little ambiguity except possibly for γ very nearly unity.

Turbulent zone averages of quantities associated with u, v and θ were obtained with the P.A.R. box car integrator, integration being carried out during those time intervals for which the gate was triggered by $I(t)$. When determining high-order zone averages of moments of $q-\overline{q}_t$, $\overline{q}_t$ was first subtracted from q using potentiometers and dual-summer amplifiers on the E.A.I. 180 analog computer before applying $(q-\overline{q}_t)^n$ to the box car integrator. In the determination of the skewness and flatness factors of $q-\overline{q}_t$, three multipliers were used, the output from each amplifier being checked and sometimes conditioned (particularly at low values of γ) to avoid overloading of the next multiplier stage.

4. Results and discussion

4.1. *Intermittency results*

Mean velocity and temperature defect profiles obtained for different x/d for the three values of the ratio U_j/U_1 are similar when L_0, U_0 and T_0 are used as the relevant length, velocity and temperature scales respectively. L_0 is taken as the distance from the axis to the position where $T-T_1 = \frac{1}{2}T_0$, where T_0 is the difference between the temperature on the axis and T_1. U_0 is the difference between the velocity on the axis and U_1. The scales U_0 and T_0 have been used throughout this

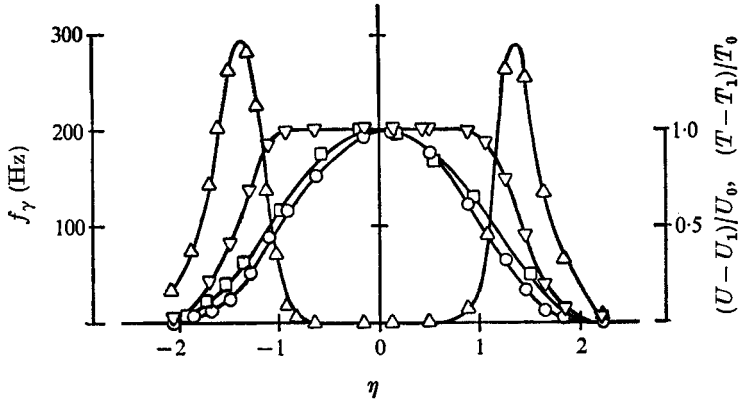

FIGURE 3. Mean velocity, mean temperature, γ and f_γ distributions across the jet ($x/d = 59$, $U_j/U_1 = 1{\cdot}9$). △, f_γ; ▽, γ; □, $(T-T_1)/T_0$; ○, $(U-U_1)/U_0$.

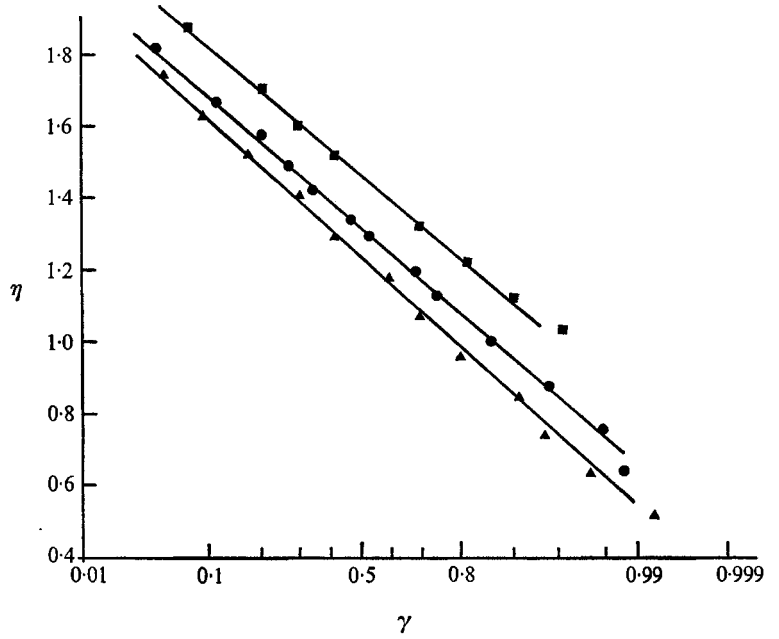

FIGURE 4. Intermittency factor γ for different U_j/U_1 (probability scale). ▲, $U_j/U_1 = 6{\cdot}6$; ●, $U_j/U_1 = 2{\cdot}9$; ■, $U_j/U_1 = 1{\cdot}9$.

section to normalize both conventional and zone-averaged velocities and temperatures. The mean velocity defect $f(\eta) = (U-U_1)/U_0$ (where $\eta = r/L_0$) and temperature defect $g(\eta) = (T-T_1)/T_0$, for $U_j/U_1 = 1{\cdot}9$, plotted in figure 3, are closely symmetrical across the jet cross-section. These profiles are in good agreement with the similarity relations given in Antonia & Bilger (1974),† with the temperature defect extending beyond the velocity defect. The velocity scale L_u, defined as the distance from the axis to the position where $U-U_1 = \frac{1}{2}U_0$, is about $0{\cdot}84L_0$.

† The results of Antonia & Bilger (1974) were obtained with a slightly different nozzle diameter ($d = 15{\cdot}9$ mm) and slightly different initial conditions.

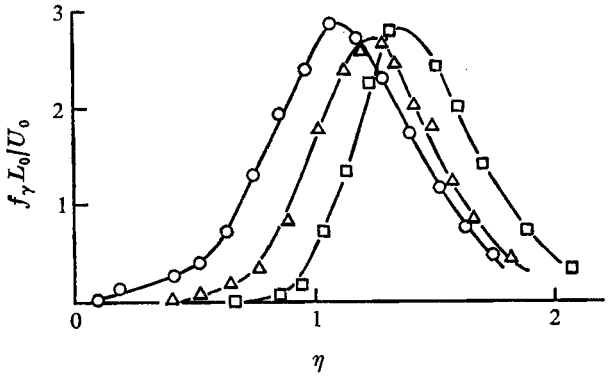

FIGURE 5. Interface frequency f_γ for different U_j/U_1.
○, $U_j/U_1 = 6{\cdot}6$; △, $U_j/U_1 = 2{\cdot}9$; □, $U_j/U_1 = 1{\cdot}9$.

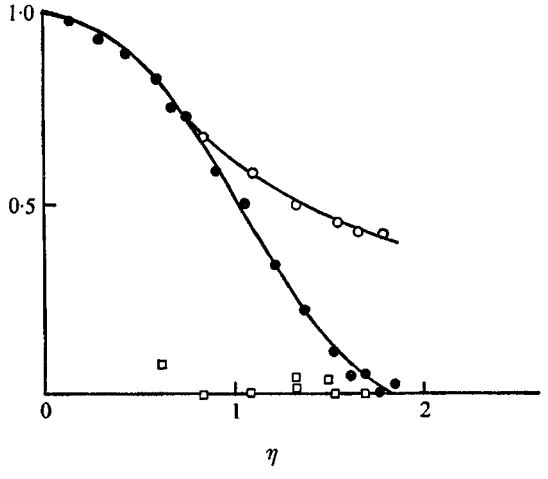

FIGURE 6. Mean temperature and zone averages ($U_j/U_1 = 6{\cdot}6$).
●, $(T-T_1)/T_0$; ○, $(T_t-T_1)/T_0$; □, $(T_n-T_1)/T_0$.

The distributions of γ and f_γ also shown in figure 3 further support the good symmetry of the jet. Profiles of γ on probability paper for the three values of U_j/U_1 are shown in figure 4 and indicate that the probability density of the interface position is closely Gaussian, except perhaps for $\gamma > 0{\cdot}9$, where the measurements are less reliable. The mean interface position, defined by the value of r at which $\gamma = \frac{1}{2}$, decreases significantly (relative to L_0) as U_j/U_1 is increased but the standard deviation is almost unchanged, being approximately equal to $\frac{1}{3}L_0$. The systematic variation of γ (figure 4) with U_j/U_1 reinforces the conclusion of Antonia & Bilger (1973) that, although the mean velocity (and temperature) field is closely self-preserving, the turbulence structure is not self-preserving and the length scale of the turbulence as given, say, by the position of the mean interface continuously changes with respect to L_0, the length scale of the mean flow.

The interface frequency, plotted in figure 5 as $f_\gamma L_0/U_0$ *vs.* η, shows that the position of the peak (which corresponds roughly to $\gamma = \frac{1}{2}$) is increased relative to

	Jet, present results, $U_j/U_1 = 6{\cdot}6$			Mixing layer (Fiedler 1974; Wygnanski & Fiedler 1970) low velocity side			Wake, Kovasznay & Ali (1974)	
γ	$\frac{\overline{u}_t-\overline{u}_n}{U_0}$	$\frac{\overline{v}_t-\overline{v}_n}{U_0}$	$\frac{\overline{\theta}_t-\overline{\theta}_n}{T_0}$	$\frac{\overline{u}_t-\overline{u}_n}{U_0}$	$\frac{\overline{v}_t-\overline{v}_n}{U_0}$	$\frac{\overline{\theta}_t-\overline{\theta}_n}{T_0}$	$\frac{\overline{u_t}-\overline{u_n}}{U_0}$	$\frac{\overline{\theta_t}-\overline{\theta_n}}{T_0}$
0·75	0·15	0·09	0·60	0·16	0·03	0·30	0·20	0·43
0·50	0·11	0·08	0·48	0·15	0·02	0·26	0·16	0·40
0·25	0·06	0·07	0·13	0·16	0·01	0·20	0·16	0·40

TABLE 1. Differences between zone-averaged mean velocities and temperatures in various shear flows

L_0 as the velocity ratio is decreased. It is important that some allowance be made in calculation methods to include the correct development of the turbulence length scale in this flow. The magnitude of the peak in figure 5 is approximately 2·8 for the three values of U_j/U_1.

4.2. *Zone-averaged velocities and temperatures*

The zone-averaged values of a fluctuating quantity q satisfy the relation

$$\gamma\overline{q}_t + (1-\gamma)\,\overline{q}_n = 0$$

when the conventional average of q is made zero. The turbulent zone average $\overline{\theta}_t$ of the temperature fluctuation is shown in figure 6 added on to the mean temperature defect $\Delta T/T_0$. The value of $T_t\,(=T+\overline{\theta}_t)$ is considerably higher than the local mean temperature T in the outer part of the flow. The value of $T_n\,(=T+\overline{\theta}_n)$ is, not unexpectedly, approximately equal to T_1, since the irrotational fluid remains at the ambient temperature. The positive values of $T_n - T_1$ reported in the intermittent region of a two-dimensional wake (Kovasznay & Ali 1974) and on the low velocity side of a mixing layer (Fiedler 1974) can only be assumed to be in error.

It is noticeable that the values of $(\overline{\theta}_t-\overline{\theta}_n)/T_0$ (figure 6) are considerably larger than the corresponding differences $(\overline{u}_t-\overline{u}_n)/U_0$ (figure 7) and $(\overline{v}_t-\overline{v}_n)/U_0$ (figure 8) between the zone-averaged velocities. These differences are given in table 1 for three values of γ (0·25, 0·5 and 0·75) and compare favourably with those obtained in wakes and mixing layers.† The mean velocity V shown in figure 8 was calculated using the continuity equation and the value of dL_0/dx was obtained from the relation

$$T_0 L_0^2 \int_0^\infty g(u_1 + u_0 f)\,\eta\,d\eta = \text{constant},$$

† It is easy to show that the maximum value of $|\overline{\theta}_t-\overline{\theta}_n|$ is $\leqslant \overline{(\theta^2)}^{\frac{1}{2}}/[\gamma(1-\gamma)]^{\frac{1}{2}}$. As $\overline{(\theta^2)}^{\frac{1}{2}}/T_0$ in the outer part of the jet is significantly larger see (§ 4.3) than $\overline{(u^2)}^{\frac{1}{2}}/U_0$, the bounds on $(\overline{\theta}_t-\overline{\theta}_n)/T_0$ would seem less tight than those for $(\overline{u}_t-\overline{u}_n)/U_0$ or $(\overline{v}_t-\overline{v}_n)/U_0$.

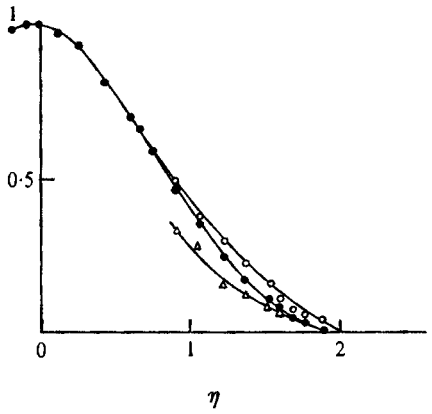

FIGURE 7. Mean axial velocity and zone averages ($U_1/U_1 = 6{\cdot}6$).
●, $(U-U_1)/U_0$; ○, $(U_t-U_1)/U_0$; △, $(U_n-U_1)/U_0$.

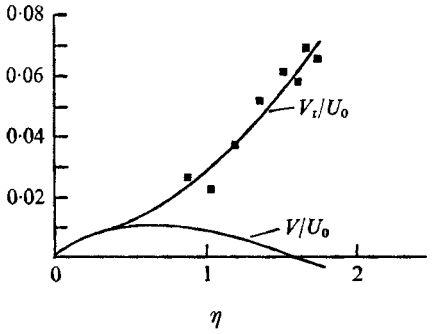

FIGURE 8. Mean radial velocity and zone averages ($U_1/U_1 = 6{\cdot}6$).
—, calculated V/U_0; ■, V_t/U_0.

which expresses the constancy of heat flux across all planes perpendicular to the flow axis. The variation of U_0 and T_0 was found by Antonia & Bilger (1974) to be proportional to x^{-1}. Although the values of V are only small, the values of V_t are large compared with V and increase appreciably near the outer edge of the jet, emphasizing the importance of the radial velocity fluctuations in the turbulent regions of the flow.

4.3. *Zone-averaged fluctuation levels*

Conventional r.m.s. fluctuations in temperature are shown in figure 9 in the form $(\overline{\theta^2})^{\frac{1}{2}}/T_0$ *vs.* η. The peak intensity occurs near $\eta = 1$ whilst the value at the axis is slightly larger than the value of 0·18 obtained by Wilson & Danckwerts (1964) in a self-preserving round jet with a quiescent free stream. This increase in $(\overline{\theta^2})^{\frac{1}{2}}/T_0$ is in qualitative agreement with the trend indicated in Antonia & Bilger (1974). Turbulent zone averages of the mean-square temperature fluctuations are also shown in figure 9, as $(\overline{\theta_t^2})^{\frac{1}{2}}/T_0$, where θ_t is measured with respect to the conventional mean value of θ, which was made zero. The values of $(\overline{\theta_t^2})^{\frac{1}{2}}/T_0$ rise less

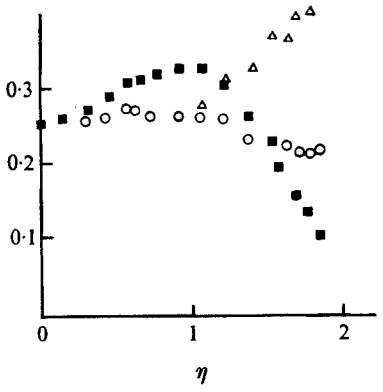

FIGURE 9. Conventional and conditional r.m.s. temperature fluctuations.
■, $(\overline{\theta^2})^{\frac{1}{2}}/T_0$; △, $(\overline{\theta_t^2})^{\frac{1}{2}}/T_0$; ○, $[\overline{(\theta-\theta_t)_t^2}]^{\frac{1}{2}}/T_0$.

sharply than those of $(\overline{\theta^2})^{\frac{1}{2}}/T_0$ in the inner region of the jet but continue to increase in the outer region of the flow, whilst $(\overline{\theta_t^2})^{\frac{1}{2}}/T_0$ decreases monotonically. The rise in $\overline{\theta_t^2}$ in the outer region appears to be reasonable when the relation

$$\overline{\theta^2} = \gamma\overline{\theta_t^2} + (1-\gamma)\,\overline{\theta_n^2}$$

is considered as the contribution from $\overline{\theta_n^2}$ ($\equiv \overline{\theta_n^2}$) is small as $\gamma \to 0$ whilst $\overline{\theta^2}$ remains finite. The mean-square value of the turbulent fluctuations measured with respect to the zone average $\overline{\theta}_t$ is also given in figure 9. The value of

$$[\overline{(\theta-\theta_t)_t^2}]^{\frac{1}{2}}/T_0$$

does not change appreciably across the jet. This value is related to $\overline{\theta^2}$ by

$$\overline{\theta^2} = \gamma\overline{(\theta-\theta_t)_t^2} + \gamma(1-\gamma)\,(\overline{\theta}_t - \overline{\theta}_n)^2,$$

which is closely confirmed by the experimental data.

The values of $(\overline{u^2})^{\frac{1}{2}}/U_0$ and $(\overline{v^2})^{\frac{1}{2}}/U_0$ (figures 10 and 11) on the jet axis are slightly higher than those of $(\overline{\theta^2})^{\frac{1}{2}}/T_0$ whilst the peak in the $(\overline{\theta^2})^{\frac{1}{2}}/T_0$ distribution is no longer distinct in either the $\overline{u^2}$ or $\overline{v^2}$ distributions. The values of $\overline{u_t^2}$ and $\overline{v_t^2}$ decrease in the outer region of the jet and there is little appreciable difference between these values and the corresponding quantities $(u-\overline{u}_t)_t^2$ and $(v-\overline{v}_t)_t^2$. The relation between the zone-averaged mean-square velocity fluctuations is

$$\overline{u^2} = \gamma\overline{(u-\overline{u}_t)_t^2} + (1-\gamma)\,\overline{(u-\overline{u}_n)_n^2} + \gamma(1-\gamma)\,(\overline{u}_t - \overline{u}_n)^2,$$

and although the contribution from the third term on the right-hand side is small the value of $\overline{(u-\overline{u}_n)_n^2}$ can be as high as that of $\overline{(u-\overline{u}_t)_t^2}$.

The values of the Reynolds shear stress $\overline{uv}$ and the heat fluxes $\overline{u\theta}$ and $\overline{v\theta}$ are presented in figures 12–14. These distributions all peak near $\eta = 0{\cdot}8$ but the magnitude of this peak is slightly underestimated by the calculations of $\overline{uv}/U_0^2$

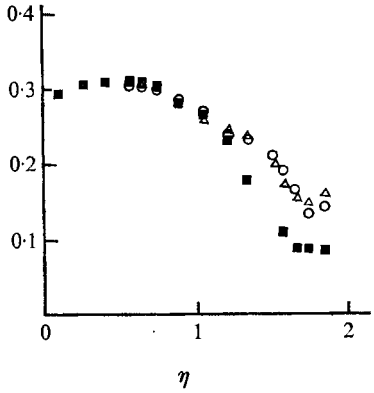

FIGURE 10. Conventional and conditional r.m.s. axial velocity fluctuations. ■, $(\overline{u^2})^{\frac{1}{2}}/U_0$; △, $(\overline{u_t^2})^{\frac{1}{2}}/U_0$; ○, $[\overline{(u-\overline{u}_t)_t^2}]^{\frac{1}{2}}/U_0$.

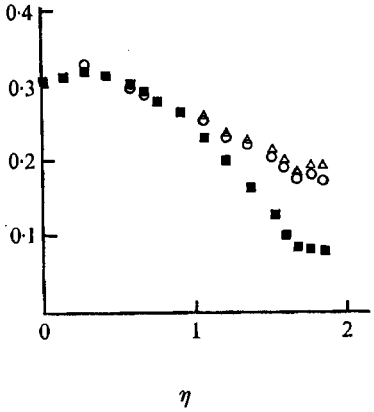

FIGURE 11. Conventional and conditional r.m.s. radial velocity fluctuations. ■, $(\overline{v^2})^{\frac{1}{2}}/U_0$; △, $(\overline{v_t^2})^{\frac{1}{2}}/U_0$; ○, $[\overline{(v-\overline{v}_t)_t^2}]^{\frac{1}{2}}/U_0$.

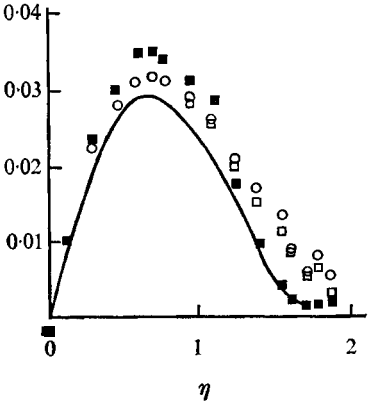

FIGURE 12. Conventional and zone averages of Reynolds shear stress uv. —, calculated $\overline{uv}/U_0^2$. Experiment: ■, $\overline{uv}/U_0^2$; ○, $(\overline{uv})_t/U_0^2$; □, $\overline{(u-\overline{u}_t)(v-\overline{v}_t)_t}/U_0^2$.

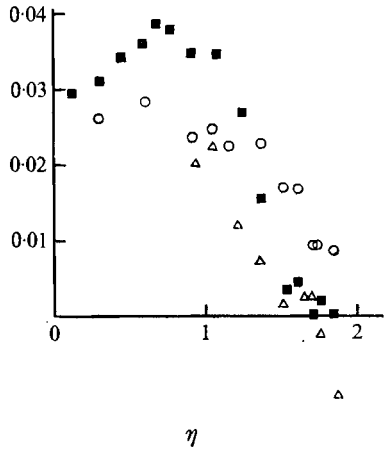

FIGURE 13. Conventional and zone averages of Reynolds heat flux $u\theta$.
■, $\overline{u\theta}/U_0T_0$; ○, $(\overline{u\theta})_t/U_0T_0$; △, $\overline{(u-\overline{u}_t)\,(\theta-\overline{\theta}_t)_t}/U_0T_0$.

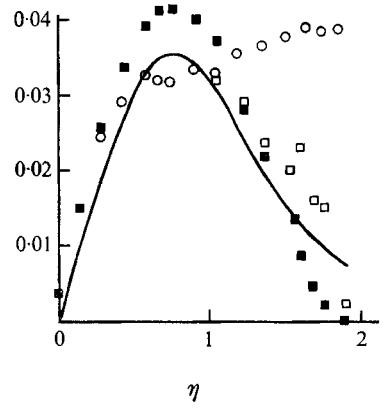

FIGURE 14. Conventional and zone averages of Reynolds heat flux $v\theta$.
Experiment: ■, $\overline{v\theta}/U_0T_0$; ○, $(\overline{v\theta})_t/U_0T_0$; □, $\overline{(v-\overline{v}_t)\,(\theta-\overline{\theta}_t)_t}/U_0T_0$.

and $\overline{v\theta}/U_0T_0$, which assumed self-preservation of the mean velocity and temperature profiles.† The zone-averaged quantities $(\overline{uv})_t$, $(\overline{u\theta})_t$ and $(\overline{v\theta})_t$ deviate from the corresponding conventional averages at $\eta \simeq 0{\cdot}3$. The Reynolds stress $(\overline{uv})_t$ is slightly lower than $\overline{uv}$ for $\eta < 1$ but this trend is, not unexpectedly, reversed for $\eta > 1$. A more dramatic result, however, is the difference in the behaviour of $(\overline{v\theta})_t$ and $(\overline{u\theta})_t$ in the intermittent region of the flow. Whereas the former continues to increase with increasing η, the latter decreases continuously. This result is consistent with the increased importance of the radial v_t fluctuations for large η and suggests that most of the transport of temperature fluctuations to the outer region is by these radial fluctuations.

† For details of these calculations see Antonia & Bilger (1974).

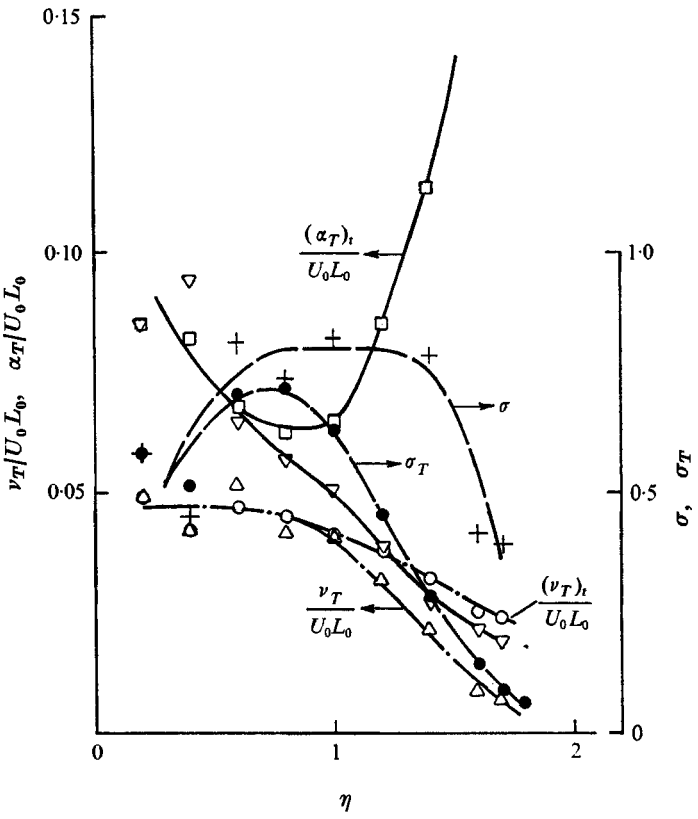

FIGURE 15. Distributions of momentum, thermal diffusivities and turbulent Prandtl number. Momentum diffusivity ν_T/U_0L_0: △, conventional; ○, turbulent zone. Thermal diffusivity α_T/U_0L_0: ▽, conventional; □, turbulent zone. Turbulent Prandtl number σ: +, conventional; ●, turbulent zone.

The turbulent eddy viscosity, defined as

$$\nu_T = \frac{-\overline{uv}}{\partial U/\partial r},$$

is shown in figure 15. The value of ν_T/U_0L_0 appears to be constant (about 0·05) in the inner part of the flow but decreases rapidly for $\eta > 1$. The value 0·05 corresponds to a Reynolds number U_0L_0/ν_T of 20, which is considerably lower than the value of 45 inferred from Wygnanski & Fiedler's (1969) measurements in a self-preserving jet in still air. The eddy viscosity in the turbulent part of the flow, defined here as $-(\overline{uv})_t/(\partial U_t/\partial r)$, is only slightly higher than ν_T in the intermittent region. The thermal diffusivity $\alpha_T = \overline{v\theta}(\partial T/\partial r)^{-1}$ decreases continuously for $\eta > 0{\cdot}4$ but its turbulent part $(\alpha_T)_t$ $(= \overline{v\theta}_t(\partial T_t/\partial r)^{-1})$ shows an appreciable increase in the intermittent region, a result of the rapid increase in $\overline{v\theta}$ (figure 14) and the flattening out of the T_t profile (figure 6) in this region. The increase in $(\alpha_T)_t$ for $\eta > 1$ results in the turbulent Prandtl number in the outer part of the

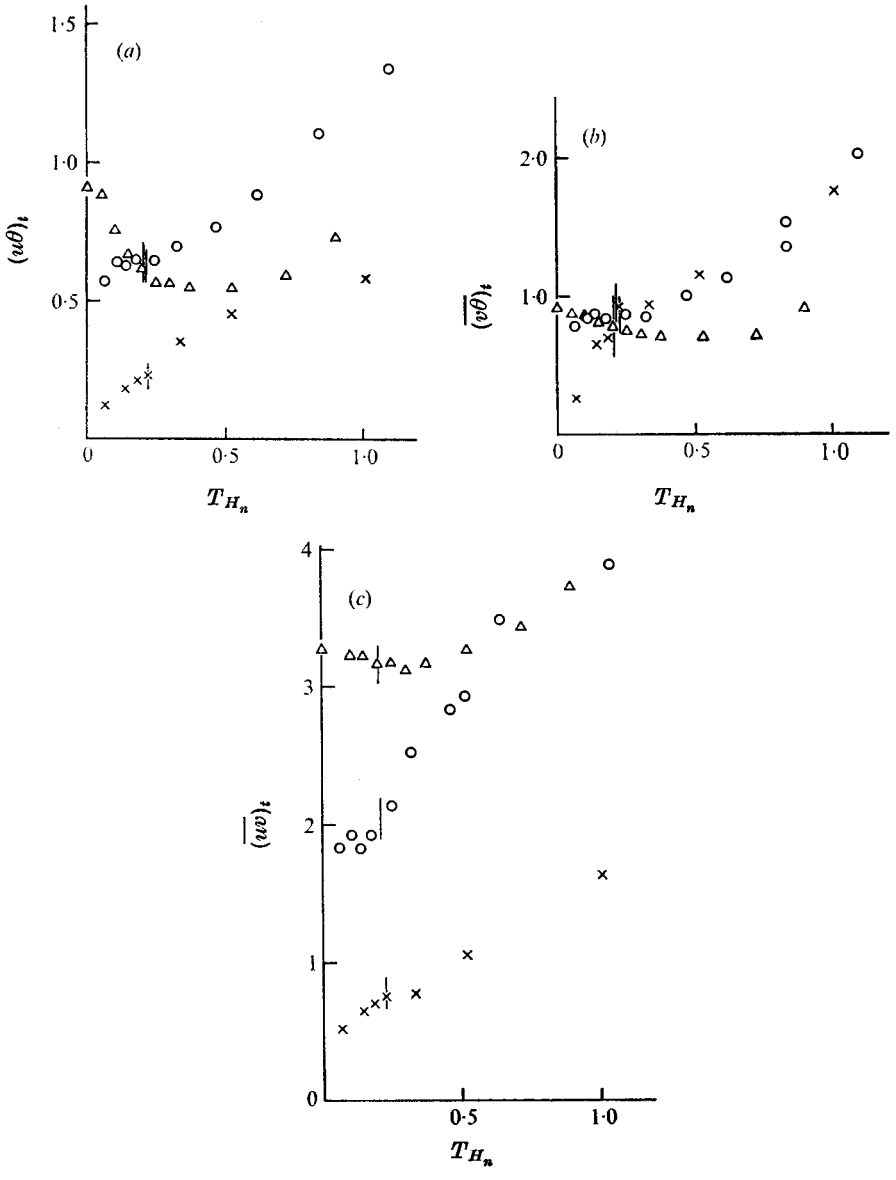

FIGURE 16. Effect of threshold T_{H_n} on (*a*) $(\overline{u\theta})_t$, (*b*) $(\overline{v\theta})_t$ and (*c*) $\overline{uv}_t$. T_{H_n} is defined as $T_H/[\overline{(\theta-\theta_n)_t^2}]^{\frac{1}{2}}$. Vertical lines indicate visual settings of T_H. ×, $\gamma = 0{\cdot}11$, $\eta = 1{\cdot}63$; ○, $\gamma = 0{\cdot}40$, $\eta = 1{\cdot}33$; △, $\gamma = 0{\cdot}88$, $\eta = 0{\cdot}89$.

flow being smaller than the conventionally defined Prandtl number σ ($= \nu_T/\alpha_T$). The value of σ for $\eta < 1$ is in the range 0·6–0·8.

The variations of the turbulent zone-averaged fluxes $(\overline{u\theta})_t$, $(\overline{v\theta})_t$ and $(\overline{uv})_t$ with the threshold setting are given in figures 16(*a*), (*b*) and (*c*) for three values of η (0·89, 1·33 and 1·63). It may be seen from these figures that these fluxes in general increase with the threshold at $\eta = 1{\cdot}63$ ($\gamma = 0{\cdot}11$). This result seems reasonable as a higher threshold swamps correlations at low fluctuation levels and weights

correlations at higher fluctuation levels of θ. The fluxes in general tend to become flat for lower values of η (higher γ) around the expected correct setting of the threshold (the vertical lines in figure 16 indicate the visual settings of the threshold). From these figures and the previous discussion of the variation of γ and f_γ with the threshold (see also figure 2), it is clear that, where the variation of these fluxes required the accurate formation of $I(t)$, it was possible to set the threshold unambiguously (figure 2 for $\gamma = 0{\cdot}11$), and where the determination of $I(t)$ was less objective, the variation of the fluxes (figure 16 for $\gamma = 0{\cdot}88$) was small, so that in both cases the errors in the measurement of zone averages were low.

5. Budget for θ^2

The equation expressing the budget for $\overline{\theta^2}$ across the jet is approximately given by

$$U\frac{\partial\overline{\theta^2}}{\partial x} + V\frac{\partial\overline{\theta^2}}{\partial r} + r^{-1}\frac{\partial}{\partial r}(r\overline{v\theta^2}) + 2\overline{v\theta}\frac{\partial T}{\partial r} + \epsilon_\theta = 0,$$

where the dissipation term due to the thermal diffusivity has been neglected. The terms of this equation non-dimensionalized by using the scales U_0, L_0 and T_0 are shown in figure 17. The first two terms, which represent the advection of $\overline{\theta^2}$ by the mean flow, have been calculated by assuming similarity of the mean velocity field and representing the distribution of $\overline{\theta^2}$ across the jet by $\overline{\theta^2} = T_0^2 g_1(\eta)$, where it should be emphasized that $g_1(\eta)$ is not universal, but a function of U_j/U_1. The third term, the diffusion of θ^2, derived from the $\overline{\theta^2 v}$ distribution (figure 18), is positive near the axis and the outer edge of the jet. The production term is almost symmetrical with respect to $\eta = 0{\cdot}9$. The dissipation ϵ_θ was obtained by assuming isotropy, i.e. $\epsilon_\theta = 6\alpha\overline{(\partial\theta/\partial x)^2}$ and $\overline{(\partial\theta/\partial x)^2}$ was inferred from the value of $\overline{(\partial\theta/\partial t)^2}$ by assuming Taylor's hypothesis. Although measurements in both this flow and various atmospheric shear flows of the skewness of the temperature derivative have confirmed the anisotropy of the small-scale temperature fluctuations (e.g. Antonia & Van Atta 1975) it is unlikely that this anisotropy is reflected in the second-order moments of the temperature derivatives. Freymuth & Uberoi (1971) showed that, in a two-dimensional heated wake,

$$\overline{(\partial\theta/\partial x)^2} = \overline{(\partial\theta/\partial y)^2} = \overline{(\partial\theta/\partial z)^2}$$

to a very close approximation.† Near the edge of the jet ($\eta \simeq 1{\cdot}8$), the dissipation is, like the production, very nearly zero but the non-zero advection and diffusion terms are approximately in balance.

The budget of $\overline{\theta^2}$ fluctuations in the turbulent zone was calculated from the zone-average measurements and is also shown in figure 17. The dissipation rate in the turbulent zone is almost constant across the flow.‡ (A similar result was

† The validity of this isotropic relation for an axisymmetric jet is currently being checked.

‡ The constant value of $(\overline{\epsilon_\theta})_t$ and the fact that $\overline{(\partial\theta/\partial x)^2} = 0$ in the non-turbulent part of the flow suggest that the assumptions inherent in Townsend's (1956, p. 145) proposal for determining γ from the flatness factor of the velocity derivative might prove to be closely satisfied if the properties of the temperature derivative were considered.

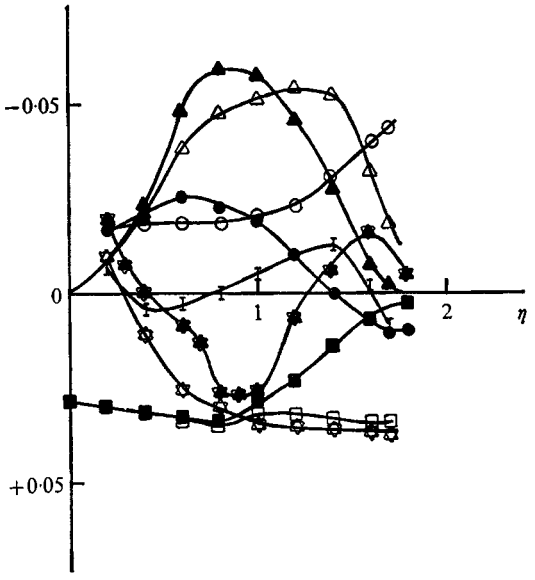

FIGURE 17. Conventional and turbulent budgets of $\overline{\theta^2}$. Closed symbols, conventional averages; open symbols, turbulent averages. ▲, production; ●, advection; ★, diffusion; ■, dissipation; I, imbalance for turbulent budget.

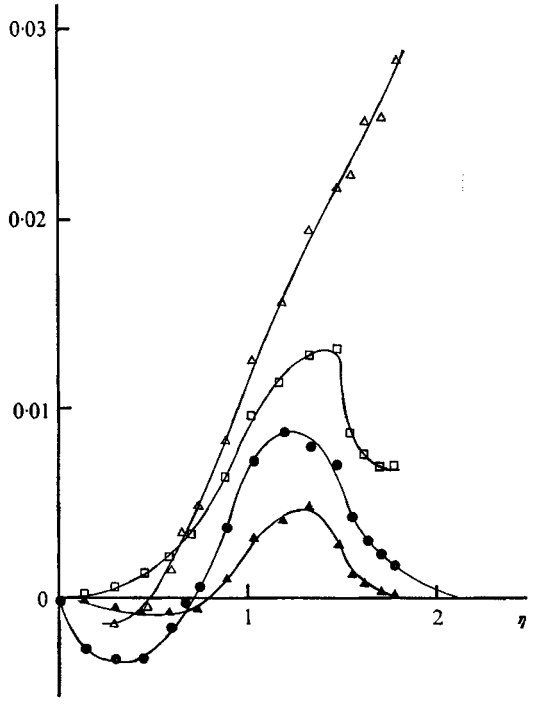

FIGURE 18. Conventional and turbulent zone averages of $\overline{\theta^2 v}$ and $\overline{\theta^2 u}$. ▲, $\overline{\theta^2 u}/U_0 T_0^2$; □, $(\overline{\theta^2 u})_t/U_0 T_0^2$; ●, $\overline{\theta^2 v}/U_0 T_0^2$; △, $(\overline{\theta^2 v})_t/U_0 T_0^2$.

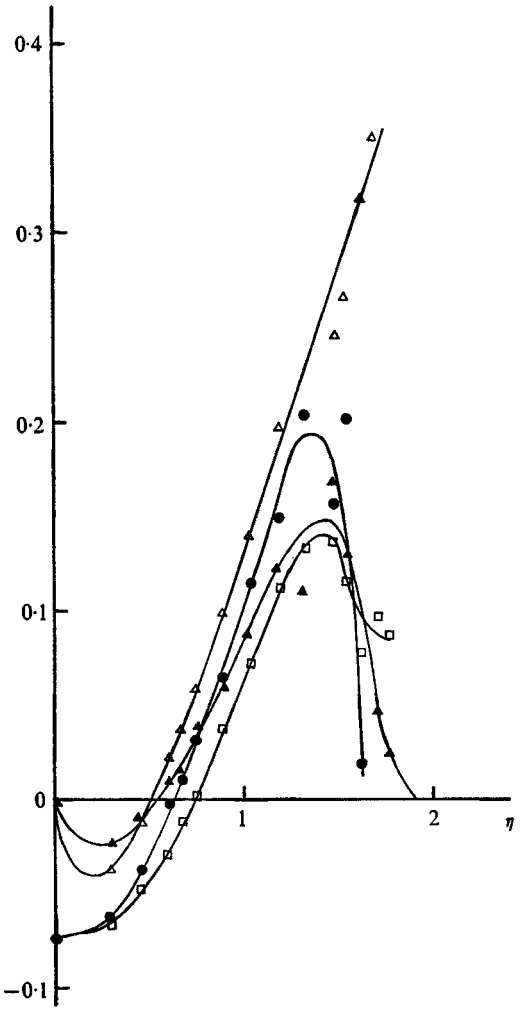

FIGURE 19. Perturbation of convection velocities of turbulent energy in the axial and radial directions. ●, $\overline{(u^2+v^2)\,u}/\overline{(u^2+v^2)}U_0$; □, $\overline{[(u^2+v^2)\,u]_t}/\overline{(u^2+v^2)_t}U_0$; ▲, $\overline{(u^2+v^2)\,v}/\overline{(u^2+v^2)}U_0$; △, $\overline{[(u^2+v^2)\,v]_t}/\overline{(u^2+v^2)_t}U_0$.

obtained by Wygnanski & Fiedler (1970) for the dissipation of velocity fluctuations on the low velocity side of a plane mixing layer.) In the outer part of the jet, the diffusion remains negative and roughly equal to the dissipation, so that there is no longer transport of $\overline{\theta^2}$ by diffusion from the region where $\overline{\theta^2}$ is largest to the outer, low temperature side of the flow. To compensate for the loss by diffusion in the outer part of the flow, the advection continues to rise in this region and exceeds the production term for $\eta > 1{\cdot}6$. The amount by which the measured budget of $\overline{\theta^2}$ in the turbulent region fails to close can only be considered as satisfactory. We have no explanation for the larger magnitude of the imbalance in the case of the conventional budget apart from the doubt relating to the assumption of isotropy in deriving the conventional ϵ_θ.

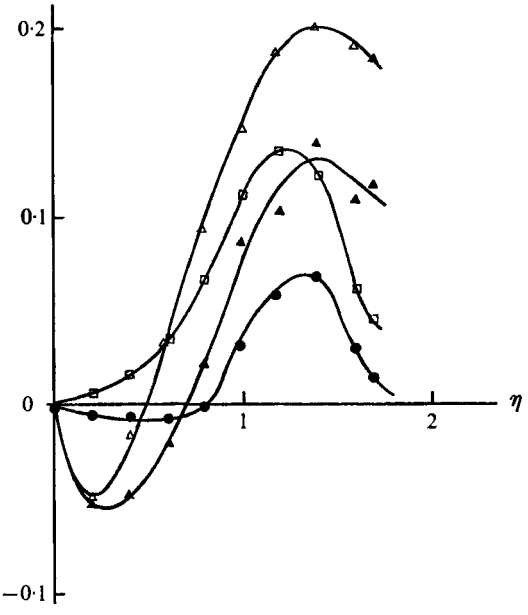

FIGURE 20. Perturbation of convection velocities of $\overline{\theta^2}$ in the axial and radial directions. ▲, $\overline{\theta^2 v}/\overline{\theta^2}U_0$; △, $(\overline{\theta^2 v})_t/\overline{\theta^2_t}U_0$; ●, $\overline{\theta^2 u}/\overline{\theta^2}U_0$; □, $(\overline{\theta^2 u})_t/\overline{\theta^2_t}U_0$.

An interesting feature of the lateral rate of transport of $\overline{\theta^2}$ in figure 18 is the almost linear increase in $(\overline{\theta^2 v})_t$ in the intermittent part of the flow. The magnitude of $(\overline{\theta^2 v})_t$ is large compared with $(\overline{\theta^2 u})_t$ in the outer part of the flow. The distribution of $\overline{\theta^2 v}$ changes sign at $\eta \simeq 0{\cdot}7$ and appears to be qualitatively (at least) correlated with the gradient of $\overline{\theta^2}$ in the radial direction. The shape of $\overline{\theta^2 v}$ is qualitatively similar to that obtained by Freymuth & Uberoi (1971) in a two-dimensional wake but different to that measured by the same authors in an axisymmetric wake (Freymuth & Uberoi 1973), where $\overline{\theta^2 v}$ is positive everywhere in the flow.

A bulk convection velocity for the flow has been defined by Townsend as $\overline{q^2 v}/\overline{q^2}$,† where $\overline{q^2}$ is the turbulent energy $\overline{u^2}+\overline{v^2}+\overline{w^2}$ and w is the fluctuation in the azimuthal direction. This convection velocity is loosely approximated in figure 19 by $\overline{(u^2 v+v^3)}/(\overline{u^2}+\overline{v^2})$ as w was not measured in this experiment. The term $\overline{(u^2+v^2)u}/(\overline{u^2}+\overline{v^2})$, also plotted in figure 19, can be loosely equated to $\overline{q^2 u}/\overline{q^2}$, which is interpreted by Bradshaw (1966) as the difference between the convection velocity U_c and the local mean flow velocity U, provided that the correlation $\overline{pu}$ (p being the local pressure fluctuation) is negligible. The distribution of

$$\overline{(u^2+v^2)u}/\overline{(u^2+v^2)}$$

suggests that U is less than U_c for $\eta < 0{\cdot}6$ but greater than U_c for $\eta > 0{\cdot}6$, a result

† Bradshaw (1966) has shown that for a self-preserving boundary layer the propagation velocity $(\frac{1}{2}\overline{q^2 v}+\overline{pv})/\frac{1}{2}\overline{q^2}$ (with the pressure–velocity correlation $\overline{pv}$ assumed negligible) is approximately equal to the entrainment rate of the layer.

which is qualitatively similar to that obtained by Bradshaw (1966) for a mixing layer and by Wygnanski & Fiedler (1969)† in a self-preserving jet. The distribution of $\overline{(u^3+uv^2)}_t/\overline{(u^2+v^2)}_t$ (figure 19) has a lower peak value than the corresponding conventional term but tends to remain higher than the conventional value near the outer edge of the jet. $\overline{(u^2v+v^3)}_t/\overline{(u^2+v^2)}_t$ continues to increase in the outer part of the jet and is significantly higher than the corresponding conventional value. It is worth noting that in the outer turbulent part of the flow most of the energy appears to be transported in the radial direction whilst on the low velocity side of the mixing layer most of the transport occurs in the axial direction.

The ratios $\overline{(\theta^2v)}/\overline{\theta^2}$ ‡ and $\overline{\theta^2u}/\overline{\theta^2}$ (figure 20) may also be loosely interpreted as convection velocities in the radial and axial directions respectively for the θ^2 fluctuations. Although the values of $\overline{\theta^2v}/\overline{\theta^2}$ near the axis of the jet are slightly more negative than those of $\overline{(u^2v+v^3)}/\overline{(u^2+v^2)}$, the values of $\overline{\theta^2u}/\overline{\theta^2}$ suggest that the convection velocity for θ^2 in the central part of the flow is closer to the mean velocity than is the convection velocity associated with the turbulent energy fluctuations. The values of $\overline{(\theta^2v)}_t/\overline{\theta^2_t}$ in the outer part are larger than those of $\overline{(\theta^2u)}_t/\overline{\theta^2_t}$ but still low compared with $\overline{(u^2v+v^3)}_t/\overline{(u^2+v^2)}_t$. The bulk convection velocity as defined by this last term is considerably higher than the conditional radial velocity $\bar{v}_t$ (or V_t). The discrepancy near the edge of the jet is considerably larger than that shown by Townsend (1956, p. 148) at the outer edge of a wake or by Wygnanski & Fiedler (1970) near the low velocity edge of a mixing layer.

6. Skewness and flatness factors of u, v and θ

The skewness $S_q \equiv \overline{q^3}/\overline{(q^2)}^{\frac{3}{2}}$ and flatness factor $F_q \equiv \overline{q^4}/\overline{(q^2)}^2$ of the instantaneous quantity q for q equal to u, v or θ are shown in figures 21–23. The flatness factor of u is very close to the Gaussian value of 3 in the region $0 < \eta < 1$ but it increases sharply in the outer part of the jet. The maximum recorded value for F_u is about 15, for $\eta = 1{\cdot}62$, but for the larger values of η, F_u decreases again, presumably down to the value of 3 characteristic of the free-stream turbulence. The conditional flatness factor of u in the turbulent zone, defined here as

$$\overline{(u-u_t)^4_t}/\overline{[(u-u_t)^2_t]}^2,$$

shows a significant increase above 3 only for $\eta > 1{\cdot}4$, and reaches a maximum value of 5 near $\eta = 1{\cdot}8$. Although conditional flatness factors of $u-\bar{u}$ in the

† We are referring here to the convection velocity inferred by these authors from the envelope of their two-point space–time correlation curves.

‡ Near the edge of a free shear layer or a turbulent boundary layer, the advection of $\overline{\theta^2}$ is nearly equal to the diffusion of $\overline{\theta^2}$ (the production and dissipation terms are negligibly small in this region). Bradshaw's (1966) analysis for a self-preserving layer, which leads to the entrainment rate of the layer being approximated to $\overline{q^2v}/\overline{q^2}$, yields an entrainment velocity approximately equal to $\overline{\theta^2v}/\overline{\theta^2}$ when it is applied to the equation for $\overline{\theta^2}$. The advantage of the latter result is that the pressure–velocity correlation does not appear in the $\overline{\theta^2}$ equation.

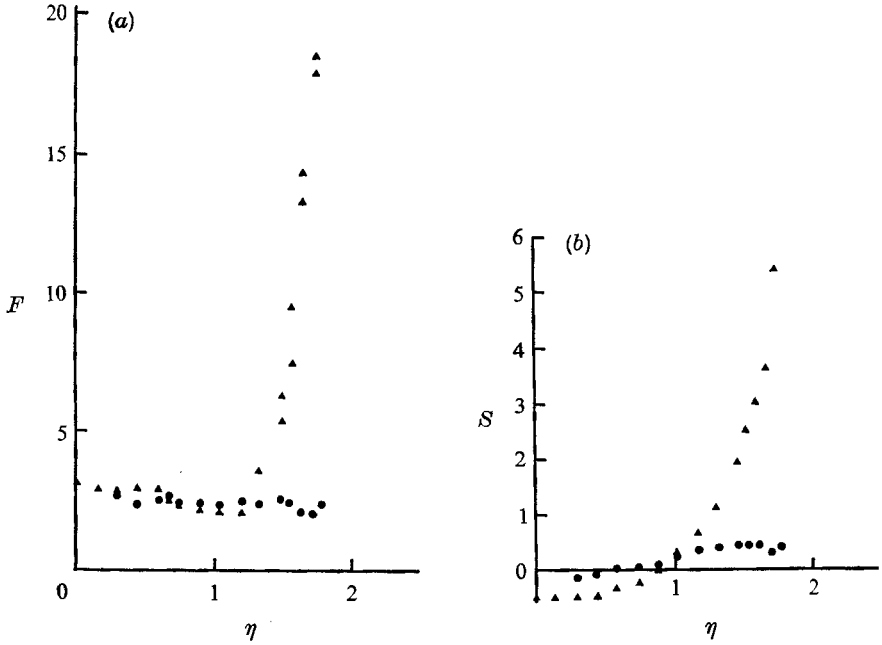

FIGURE 21. Conventional and conditional skewness and flatness factor of θ. (*a*) Flatness factor. (*b*) Skewness. ▲, $\theta-\overline{\theta}$; ●, $(\theta-\overline{\theta}_t)_t$.

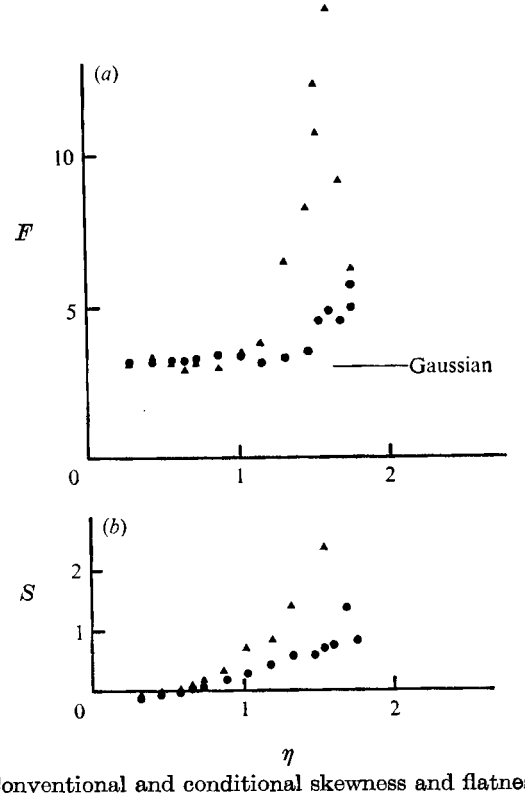

FIGURE 22. Conventional and conditional skewness and flatness factor of u. (*a*) Flatness factor. (*b*) Skewness. ▲, $u-\overline{u}$; ●, $(u-\overline{u_t})_t$.

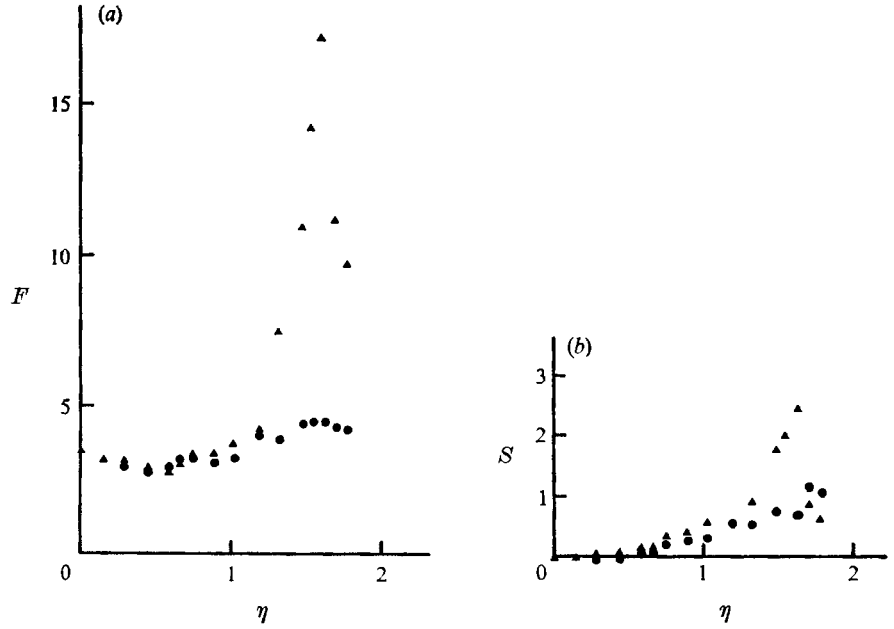

FIGURE 23. Conventional and conditional skewness and flatness factor of v. (a) Flatness factor. (b) Skewness. ▲, $v-\bar{v}$; ●, $(v-\bar{v}_t)_t$.

turbulent zone were not measured it is unlikely that they are significantly different from the conditional results of figure 21 in view of the small difference that exists between U and U_t (figure 7). The skewness S_u is almost zero near the axis (the small negative values near $\eta = 0$ are reproducible and supported by other measurements obtained with a single hot wire†) and rises to a value of 2·5 in the outer part of the jet. The skewness of $u-u_t$ in the turbulent zone also rises as η increases but at a rate slower than that of the conventional skewness. The skewness and flatness factor of v (figure 22) follow the features of S_u and F_u quite closely.

The distributions of S_θ and F_θ show significant differences from those of the skewness and flatness factors of the axial and radial velocity fluctuations. The flatness factor of θ is very close to 3 near the axis but decreases to a value of 2 near $n = 1$ before sharply increasing in the outer region. The maximum value of F_θ ($\simeq 26$ at $\eta = 1{\cdot}8$) is considerably higher than the measured peaks in the F_u and F_v distributions. The decrease in F_θ towards a value of 2 near $\eta = 1$ was also observed at different x stations and for different values of U_j/U_1. A similar trend in F_θ was noted by Fiedler (1974) in a heated two-dimensional mixing layer (the higher velocity stream was heated whilst the external stream had zero velocity and was at the ambient temperature). Fiedler suggested that the value of 2 was characteristic of the 'sawtooth' appearance of the temperature signals near the central region of the mixing layer. The sawtooth or ramp-like character of the

† Wygnanski & Fiedler (1969) obtained slightly positive values near the axis of a jet with a quiescent free stream.

temperature was also observed in this flow, in the region $0{\cdot}6 < \eta < 1{\cdot}2$ (see next section).

The flatness factor of $\theta - \theta_t$ in the turbulent zone is remarkably constant ($\simeq 2{\cdot}5$) throughout the outer, intermittent region. This result complements the nearly constant value of $\overline{(\theta-\theta_t)^2}_t$ (figure 9) and provides further support for the homogeneity of temperature fluctuations in the turbulent zone, at least when they are considered with respect to their own zone average. Values of S_θ well in excess of those for S_u and S_v are obtained in the strongly intermittent part of the flow. A similar trend may be observed in measurements in a mixing layer (Fiedler 1973) and a heated boundary layer (Fulachier 1972) and is likely to be a result of the distinct contrast between the values of θ in the irrotational ($\theta = 0$) and turbulent regions of the flow. On the other hand, the measured conditional skewness of $\theta - \theta_t$ appears to be smaller than the conditional skewness of $u - u_t$ or $v - v_t$.

7. Discussion of results

Oscilloscope traces of velocity and temperature fluctuations are shown in figures 24(*a*) ($\eta = 1{\cdot}33$) and (*b*) ($\eta = 0{\cdot}89$) (plate 1). Also shown in these figures are the instantaneous momentum flux and the intermittency function $I(t)$ derived from the temperature signal θ. The main feature of the θ trace in figure 24(*a*) is the ramp-like structure of the (at least) two relatively large duration bulges.† The temperature (inverted in figure 24*a*) rises fairly sharply at the downstream end of the bulge and then gradually decreases to the ambient value at the upstream (late time) end. It should be noted however that for the shorter duration bulges of figure 24(*a*) the temperature signal is on average symmetrically distributed about the midpoint of the bulge. As an initial attempt to put these observations on a firmer quantitative basis, Antonia (1974) obtained, using a digital computer, the ensemble-average distribution of the temperature for a turbulent bulge. The ensemble average was formed by sampling each bulge at a given value of t/T, where t is the time measured from the downstream end of the bulge and T is the duration of that particular bulge. The ensemble average was then calculated by averaging over bulges whose duration fell within a selected time interval. For bulges whose duration was in the range 2–5 times the mean bulge duration $\overline{T}$ (or γf_γ^{-1}), the ramp-like structure was clearly established but, for bulges of duration less than $\overline{T}$, no ramp-like character was observed.

For the larger duration bulge (figure 24*a*) the velocity fluctuations u and v are on average clearly higher than the corresponding values in the irrotational patches. This suggests large-scale bulges, probably originating from the central part of the jet, with an excess of momentum and with a radial velocity towards the outer flow region. This large-scale motion has the vorticity of the main flow

† The extent of a turbulent patch indicated by the θ traces appears to extend slightly beyond that indicated by the u, v or uv traces. This was probably the result of the 1 mm separation between the cold wire and the centre of the X-wire, which was further out towards the edge of the jet. It is unlikely, however, that this small separation affects any of the zone-average results presented in the previous sections.

and transports heat to the outer edge of the jet. The cooler (upstream) end of the bulge also appears to coincide with a region where v is negative. This observation suggests that the entrainment of colder, irrotational fluid might also occur in this region.† In a heated-wall boundary layer, where the vorticity of the main flow is in the opposite direction to that in the jet, it is the upstream end of the bulge which is at the higher temperature (Fulachier 1972) while most of the entrainment occurs near the downstream portion of the large-scale bulges (this is clearly indicated by the ensemble-average distributions of v shown in Antonia 1972). The heated-jet results of Sunyach (1971) and the mixing-layer results of Wygnanski & Fiedler (1970) and Fiedler (1974) emphasize the transport of heat by the large-scale structure of the flow.‡

In the region of the jet where $\gamma \to 1$ the ramp-like character of the signals is clearly evident (figure 24(b), $\gamma = 0{\cdot}89$). The two temperature traces of figure 25 (plate 1) were obtained on the jet axis ($\gamma = 1$) from cold wires situated $\sim 0{\cdot}5$ mm apart. The upper signal corresponds to the time derivative of θ whilst the lower trace is the difference between the θ signals. The sharp thermal gradients in the θ trace (leading edge of the ramp) result in a significant contribution to the derivative and difference signals. The one-sided behaviour of this contribution supports the suggestion by Gibson *et al.* (1974, private communication) that the anistropy of the small-scale temperature field might be a residual effect of the large-scale temperature structure.

8. Summary of results

The main results of this investigation may be summarized as follows.

(i) The turbulent zone-averaged temperature T_t appears to decrease slowly in the outer part of the flow. The difference $(T_t - T_n)/T_0$ is considerably larger than the corresponding difference for either U or V.

(ii) The distributions of second-, third- and fourth-order moments of temperature fluctuations in the turbulent region are more or less uniform compared with the corresponding distributions of moments of u and v.

(iii) Although the shear stress $(\overline{uv})_t$ and longitudinal heat flux $(\overline{\theta u})_t$ show a decrease in the outer flow region the radial heat flux $(\overline{\theta v})_t$ continues to increase, which seems consistent with the relatively large values of $\bar{v}_t$ obtained in this region. A consequence of this behaviour of $(\overline{\theta v})_t$ is a large increase in the thermal diffusivity α_t and a decrease in the Prandtl number σ_t for the turbulent part only of the fluid. The concept of a constant eddy viscosity for the turbulent flow region is not supported by the data.

(iv) The departure from Gaussianity of the properties of, in particular, the velocity fluctuations is significant and must be included in any theoretical model which predicts the conventional moments of u and v in the intermittent region. A departure from Gaussianity has also been noted in boundary layers

† Ensemble-average distributions of v are needed to confirm this point.

‡ The spark shadow pictures of Brown & Roshko (1974) show that a mixing layer is clearly dominated by large coherent structures.

(Hedley & Keffer 1974) and in wakes (Thomas 1973; LaRue & Libby 1974*b*). The tendency for the flatness factor F_θ to decrease towards a value of 2 in the central part of the flow appears to be supported by the ramp-like character of the longer duration turbulent bulges observed in the temperature signal. This ramp-like feature has also been observed in various other turbulent shear flows and appears to be associated with large-scale motion having the vorticity of the main flow.

(v) The turbulent budget for $\overline{\theta^2}$ is characterized by an almost constant value of the dissipation of temperature fluctuations in the outer flow region, where the magnitudes of the turbulent production, advection and diffusion of $\overline{\theta^2}$ are, in general, relatively larger than the corresponding conventional quantities.

The authors are grateful to Mr H. Q. Danh for his assistance with the experimental work. The work described in this paper represents part of a programme of research supported by the Australian Research Grants Committee and the Australian Institute of Nuclear Science and Engineering.

REFERENCES

ANTONIA, R. A. 1972 Conditionally sampled measurements near the outer edge of a turbulent boundary layer. *J. Fluid Mech.* **56**, 1.

ANTONIA, R. A. 1974 The distribution of temperature in the intermittent region of a turbulent shear flow. In *Proc. 5th Int. Heat Transfer Conf., Tokyo*, vol. 2, p. 95.

ANTONIA, R. A. & ATKINSON, J. D. 1974 Use of a pseudo-turbulent signal to calibrate an intermittency measuring circuit. *J. Fluid Mech.* **64**, 679.

ANTONIA, R. A. & BILGER, R. W. 1973 An experimental investigation of an axisymmetric jet in a co-flowing air stream. *J. Fluid Mech.* **61**, 805.

ANTONIA, R. A. & BILGER, R. W. 1974 The heated round turbulent jet in a co-flowing stream. *Charles Kolling Res. Lab., Dept. Mech. Engng, University of Sydney, Tech. Note*, F-66.

ANTONIA, R. A. & VAN ATTA, C. W. 1975 On the correlation between temperature and velocity dissipation fields in a heated turbulent jet. *J. Fluid Mech.* **67**, 273.

BRADSHAW, P. 1966 The turbulence structure of equilibrium boundary layers. *Nat. Phys. Lab. Aero. Rep.* no. 1184.

BRADSHAW, P. & MURLIS, J. 1973 On the measurement of intermittency in turbulent flow. *Imp. Coll. Aero. Tech. Note*, no. 73-108.

BROWN, G. L. & ROSHKO, A. 1974 On the density effects and large structure in turbulent mixing layers. *J. Fluid Mech.* **64**, 775.

FIEDLER, H. 1974 Transport of heat across a plane turbulent mixing layer. *Adv. in Geophys.* **18**, 93.

FREYMUTH, P. & UBEROI, M. S. 1971 Structure of temperature fluctuations in the turbulent wake behind a heated cylinder. *Phys. Fluids*, **14**, 2574.

FREYMUTH, P. & UBEROI, M. S. 1973 Temperature fluctuations in a turbulent wake behind an optically heated sphere. *Phys. Fluids*, **16**, 161.

FULACHIER, L. 1972 Contribution à l'étude des analogies des champs dynamique et thermique dans une couche limite turbulente. Effet de l'aspiration. D.Sc. thesis, Institut de Mécanique Statistique de la Turbulence, Université de Provence, Marseille.

HEDLEY, T. B. & KEFFER, J. F. 1974 Some turbulent/non-turbulent properties of the outer intermittent region of a boundary layer. *J. Fluid Mech.* **64**, 645.

KOVASZNAY, L. S. G. & ALI, S. F. 1974 Structure of the turbulence in the wake of a heated flat plate. In *Proc. 5th Int. Heat Transfer Conf. Tokyo*, vol. 2, p. 99.

KOVASZNAY, L. S. G., KIBENS, V. & BLACKWELDER, R. F. 1970 Large scale motion in the intermittent region of a turbulent boundary layer. *J. Fluid Mech.* **41**, 283.

LARUE, J. C. & LIBBY, P. A. 1974*a* Temperature and intermittency in the turbulent wake of a heated cylinder. *Phys. Fluids*, **17**, 873.

LARUE, J. C. & LIBBY, P. A. 1974*b* Temperature fluctuations in the plane turbulent wake. *Phys. Fluids*, **17**, 1956.

STELLEMA, L., ANTONIA, R. A. & PRABHU, A. 1975 A constant-current resistance thermometer for the measurement of mean and fluctuating temperatures in turbulent flows. *Charles Kolling Res. Lab., Dept. Mech. Engng, University of Sydney, Tech. Note*, D-12.

SUNYACH, M. 1971 Contribution à l'étude des frontières d'écoulements turbulents libres. D.Sc. thesis, Université Claude Bernard de Lyon.

SUNYACH, M. & MATHIEU, J. 1969 Zone de mélange d'un jet plan. *Int. J. Heat Mass Transfer*, **12**, 1679.

THOMAS, R. M. 1973 Conditional sampling and other measurements in a plane turbulent wake. *J. Fluid Mech.* **57**, 549.

TOWNSEND, A. A. 1956 *The Structure of Turbulent Shear Flow.* Cambridge University Press.

WILSON, R. A. M. & DANCKWERTS, P. V. 1964 Studies in turbulent mixing. II. A hot-air jet. *Chem. Engng Sci.* **19**, 885.

WYGNANSKI, I. & FIEDLER, H. E. 1969 Some measurements in the self-preserving jet. *J. Fluid Mech.* **38**, 577.

WYGNANSKI, I. & FIEDLER, H. E. 1970 The two-dimensional mixing region. *J. Fluid Mech.* **41**, 327.

WYNGAARD, J. C. 1971 The effect of velocity sensitivity on temperature derivative statistics in isotropic turbulence. *J. Fluid Mech.* **48**, 763.

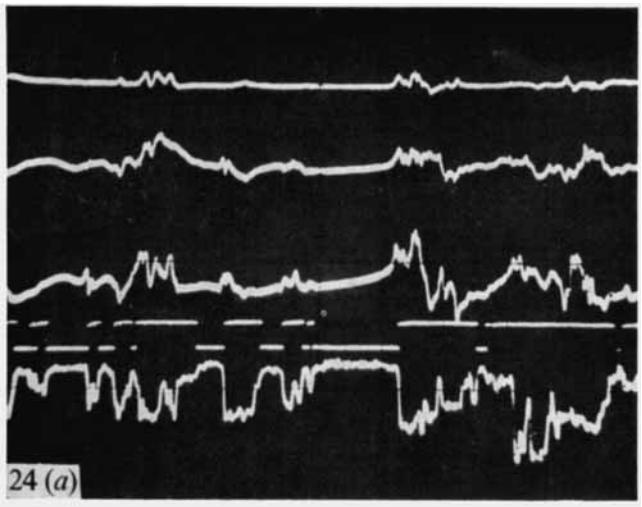

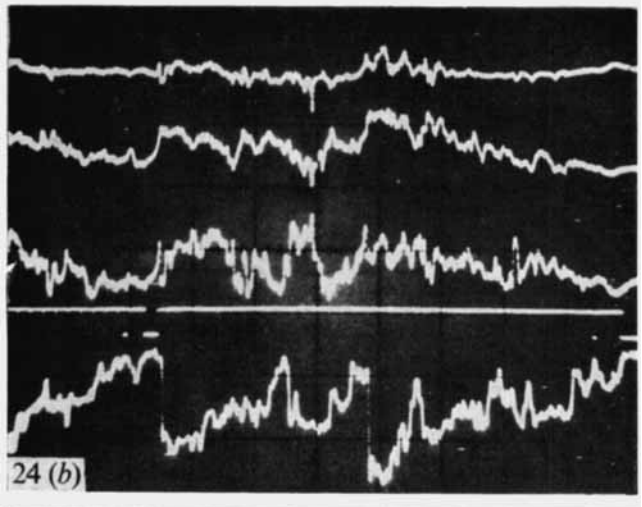

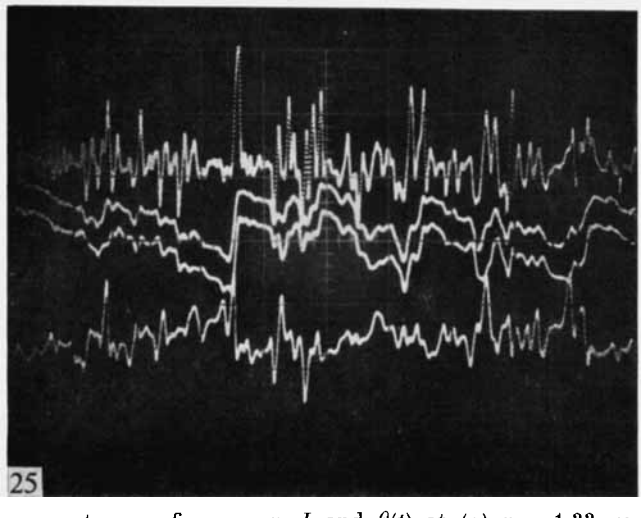

FIGURE 24. Oscilloscope traces of uv, u, v, I and $\theta(t)$ at (*a*) $\eta = 1{\cdot}33$, $\gamma = 0{\cdot}44$ and (*b*) $\eta = 0{\cdot}89$, $\gamma = 0{\cdot}88$. $U_j/U_1 = 6{\cdot}6$. The time base is 2 ms/division. The calibrations for the signals from top to bottom are uv, 20 ft^2 s^{-2}/division; u, 2 ft s^{-1}/division; v, 5 ft s^{-1}/division; $I(t)$, arbitrary; θ, 1 °C/division. Note that the $\theta(t)$ signal is inverted. Time increases to the right of the picture.

FIGURE 25. Oscilloscope traces of $\partial\theta/\partial t$, θ_1, θ_2 and $\theta_1 - \theta_2$ at the centre of the jet for $U_j/U_1 = 2{\cdot}9$. θ_1 and θ_2 are the inverted temperature signals from two cold wires separated by a distance of 0·5 mm in the r direction.